Hindawi
Mathematical Problems in Engineering
Volume 2021, Article ID 4640467, 16 pages
https://doi.org/10.1155/2021/4640467

Research Article

On the Numerical Approximation of Three-Dimensional Time Fractional Convection-Diffusion Equations

Kamran,[1] **Raheel Kamal**,[1] **Gul Rahmat**,[1] **and Kamal Shah**[2]

[1]*Department of Mathematics, Islamia College Peshawar, Peshawar, Khyber Pakhtoonkhwa, Pakistan*
[2]*Department of Mathematics, University of Malakand, Chakdara, Dir (Lower), Khyber Pakhtoonkhwa, Pakistan*

Correspondence should be addressed to Kamal Shah; kamal@uom.edu.pk

Received 12 July 2021; Revised 9 September 2021; Accepted 11 September 2021; Published 8 October 2021

Academic Editor: Ricardo Escobar

In this paper, we present an efficient method for the numerical investigation of three-dimensional non-integer-order convection-diffusion equation (CDE) based on radial basis functions (RBFs) in localized form and Laplace transform (LT). In our numerical scheme, first we transform the given problem into Laplace space using Laplace transform. Then, the local radial basis function (LRBF) method is employed to approximate the solution of the transformed problem. Finally, we represent the solution as an integral along a smooth curve in the complex left half plane. The integral is then evaluated to high accuracy by a quadrature rule. The Laplace transform is used to avoid the classical time marching procedure. The radial basis functions are important tools for scattered data interpolation and for solving partial differential equations (PDEs) of integer and non-integer order. The LRBF and global radial basis function (GRBF) are used to produce sparse collocation matrices which resolve the issue of the sensitivity of shape parameter and ill conditioning of system matrices and reduce the computational cost. The application of Laplace transformation often leads to the solution in complex plane which cannot be generally inverted. In this work, improved Talbot's method is utilized which is an efficient method for the numerical inversion of Laplace transform. The stability and convergence of the method are discussed. Two test problems are considered to validate the numerical scheme. The numerical results highlight the efficiency and accuracy of the proposed method.

1. Introduction

Fractional calculus is a fast growing field and has attracted the research community due to its applications in engineering and other sciences [1–3]. Fractional-order operators are non-local, i.e., they include the history from the initial states to the current state. Therefore, fractional operators are often applied to model systems to describe the influence of memory effects [4–6]. Fractional-order operators generalize the notion of integer-order operators [7]. Fractional-order operators can be used to model many processes such as the signal process and anomalous diffusion [8–11]. Therefore, efficient and accurate numerical methods for solving physical models involving fractional-order derivatives become an important research area [12–16].

The CDE is a mixture of the equations of diffusion and convection and explains physical phenomena in which particles, electricity, or other physical quantities are transmitted within a physical structure through two procedures: convection and diffusion. Fractional-order CDEs are regarded as the extended form of ordinary CDEs. Fractional-order CDEs can express physical problems more accurately as compared to ordinary CDEs. The fractional-order CDE has applications in many phenomena such as the mass transport [17], environmental science [18], gas transport through heterogeneous soil and gas reservoirs [19], contaminant or liquid transport in complex media and heat conduction [20], and global weather production, in which an initially discontinuous profile is propagated by diffusion and convection, the latter with a speed of c [21]. The solution of fractional-order CDE has been investigated by many authors, and they have developed many robust analytical and numerical methods in this regard. For example, the authors in [22] have studied the analytical

solution of fractional-order diffusion and convection equations. In [23], the authors have utilized the Adomian decomposition method for solving the fractional-order CDE. Momani and Yıldırım in [24] have obtained the approximate analytical solution of CDE via He's homotopy perturbation method. Since the analytical solution of fractional-order problems in most of the cases is difficult to obtain, the researchers have developed numerous numerical methods for the investigation of the solutions of fractional-order problems such as the finite difference method [25], finite element method [26], finite volume method [27], and meshless methods [28–30].

The authors in [31] studied the solution CDEs of fractional via the discontinuous Galerkin method. A box-type scheme in [32] was developed for the sub-diffusion equations of fractional order. Hristov in [33] studied the solution of fractional sub-diffusion equation via an integral method. Zhai et al. [34] proposed a compact finite difference scheme for the numerical simulation of fractional-order 3D CDE. In [8], the authors developed a numerical scheme for anomalous sub-diffusion equation. They have studied the stability and convergence of the scheme using the energy method. Chen et al. [9] proposed a numerical method with high accuracy for variable-order fractional anomalous sub-diffusion equation. They discussed the convergence and stability using Fourier analysis. In [25], a compact difference scheme was developed for the fractional-order modified anomalous sub-diffusion and wave-diffusion equations. Zeng et al. [26] solved the time fractional sub-diffusion equation by utilizing the finite difference and finite element approach. They also proposed two fully discrete schemes in [35] for the fractional sub-diffusion equation with second-order accuracy. In [36], the numerical scheme for the approximation of 2D sub-diffusion equation of fractional order was proposed. In [37], the authors proposed a numerical method for non-integer-order sub-diffusion equation. Gao and Sun [38] obtained the numerical approximation of fractional sub-diffusion equation via finite difference scheme. Hussain et al. [27] analyzed the solution of CDE numerically using the finite element method. In computational modeling, the well-known classical mesh-based methods such as finite difference, finite elements, and finite volume have received much interest in recent years. However, these algorithms were designed with constraints related to issues such as node selection and multidimensional scaling.

Recently, the meshless method has attracted more and more attention because it is among one of the powerful tools for handling PDEs. Especially the RBF-based meshless methods are one of the most popular types among these methods. The benefit of these techniques over other classical techniques such as the finite elements, finite differences, and boundary elements methods is that in these methods, no mesh or element is required for discretization of the domain or the boundary which is a difficult task especially in 3D problems. Instead, meshless methods only require a few scattered points, the connection of which is not important. In meshless methods, the refinement of mesh can easily be done with minimal cost. Meshless methods are easily extendible to multidimensional problems. Meshless methods have been proved successful for solving PDEs on both regular and irregular node arrangements. Meshless methods have been successfully applied to various engineering and other science problems. For example, in [28], a meshfree method based on finite differences was applied to diffusion equation. Oruç [11] applied the meshfree method based on finite differences for the numerical solution of Zakharov–Rubenchik equations. Dehghan and Shafieeabyaneh [29] utilized the RBF method based on finite difference to simulate the regularized long-wave equation (RLWE) and extended Fisher–Kolmogorov equation (EFKE) in higher dimensions. Mohebbi et al. [14] investigated the solution of 2D modified anomalous sub-diffusion equation of arbitrary order via the RBF method. The authors in [39] derived the error estimates of the numerical solution for reaction-sub-diffusion of fractional order via the meshless method. Wei et al. [30] obtained the numerical solution of 2D fractional-order diffusion equation based on the implicit RBF method. In [40], the authors approximated the solution of 2D fractional-order sub-diffusion equation via Kansa's method. Similarly, approximation of diffusion equation of variable fractional order with different boundary conditions based on local RBF method was carried out in [41]. Shivanian in [42] proposed an efficient local radial basis function method for the simulation of 2D fractional-order convection-diffusion reactions. The stability and convergence of the method was also proved theoretically. In [43], the numerical solutions of advection diffusion reaction equations on complex geometries using a local radial basis function method were studied. Golbabai and Kalarestaghi [44] proposed a local radial basis function method for dominated convection-diffusion equations.

However, in these time stepping schemes, the computations may be very expansive because each new iteration is dependent on the previous time step. An alternative way is to use the LT coupled with these numerical methods. In this article, we propose the LRBF method coupled with Laplace transform. The LT is used to avoid the stability restrictions, which are commonly encountered in time stepping procedures. The LRBF method is used to resolve the issue of ill conditioning of the differentiation matrices and the sensitivity of shape parameter in the GRBF method. The main idea of the LRBF method is the collocation on overlapping sub-domains of the whole domain. The overlapping subdomains remarkably reduce the size of collocation matrix by solving many small size matrices. Each small matrix has the same size as the number of nodes in the domain of influence of each node. The Caputo fractional derivatives are considered here because they allow traditional initial and boundary conditions to be included in the formulation of the problem. In this paper, we consider the linear fractional-order CDE, and the fractional derivatives are taken in Caputo sense as follows:

$$
{}_0^c D_{\mathbf{t}}^{\alpha} \mathbf{U}(\bar{\boldsymbol{\xi}}, t) = \Delta \mathbf{U}(\bar{\boldsymbol{\xi}}, t) + \mathbf{V}(\bar{\boldsymbol{\xi}}) \cdot \nabla \mathbf{U}(\bar{\boldsymbol{\xi}}, t) - \mathbf{w}(\bar{\boldsymbol{\xi}}) \mathbf{U}(\bar{\boldsymbol{\xi}}, t) + \mathbf{h}(\bar{\boldsymbol{\xi}}, t), \quad \bar{\boldsymbol{\xi}} \in \Omega,\ t > 0, \tag{1}
$$

satisfying

$$\mathbf{U}(\overline{\boldsymbol{\xi}}, 0) = \mathbf{U}_0, \quad \overline{\boldsymbol{\xi}} \in \Omega, \tag{2}$$

and

$$\mathscr{L}_b \mathbf{U}(\overline{\boldsymbol{\xi}}, t) = \mathbf{g}(\overline{\boldsymbol{\xi}}, t), \quad \overline{\boldsymbol{\xi}} \in \partial\Omega\ , \tag{3}$$

where Ω is the domain and $\partial\Omega$ is its boundary. $\mathbf{w}(\overline{\xi})$ is a function of $\overline{\xi}$ and $\mathbf{V}(\overline{\xi})$ is a vector. The forcing term $\mathbf{h}(\overline{\xi}, t)$ is sufficiently smooth and $\mathbf{g}(\overline{\xi}, t)$ and $\mathbf{U}_0$ are given continuous functions. $\mathscr{L}_b$ is the boundary differential operator, and ${}_0^c D_{\mathbf{t}}^{\alpha}\mathbf{U}(\overline{\xi}, t)$ is the Caputo fractional derivative of order α of the function $\mathbf{U}(\overline{\xi}, t)$ which is defined as

$$\begin{aligned} {}_0^c D_{\mathbf{t}}^{\alpha}\mathbf{U}(\overline{\boldsymbol{\xi}}, t) &= \frac{1}{\Gamma(\gamma - \alpha)} \int_0^t \frac{\left(\partial^{\gamma}\mathbf{U}(\overline{\boldsymbol{\xi}}, s)/\partial s^{\gamma}\right)}{(t - s)^{\alpha+1-\gamma}}\, \mathrm{d}s, \\ \gamma - 1 < \alpha < \gamma, \gamma \in \mathbb{N}, t > 0. \end{aligned} \tag{4}$$

The paper is organized as follows. In Section 2, the Laplace transform method for the given model is discussed. Section 3 describes the local RBF approximation of the transformed problem in Laplace space. Section 4 is about the stability of the discrete system. Section 5 is devoted to the approximation of inverse Laplace transform. In Section 6, the numerical scheme is applied to 3D CDE. Finally, in Section 7, the conclusion is drawn.

2. Time Discretization via Laplace Transform

Here, we apply LT to given model defined in (1)–(3) to avoid the time marching method. The LT of piecewise continuous function $U(t)$ defined on $[0, \infty)$ is defined by

$$\hat{\mathbf{U}}(s) = \mathscr{L}\{\mathbf{U}(t)\} = \int_0^{\infty} e^{-st}\mathbf{U}(t)\mathrm{d}t. \tag{5}$$

Also, the LT of the Caputo derivative ${}_0^c D_{\mathbf{t}}^{\alpha}$ is given as

$$\mathscr{L}\{{}_0^c D_{\mathbf{t}}^{\alpha}\mathbf{U}(t)\} = s^{\alpha}\hat{\mathbf{U}}(s) - \sum_{i=0}^{m-1} s^{\alpha-i-1}\mathbf{U}^{(i)}(0). \tag{6}$$

Applying the LT to equations (1)–(3), we get

$$\begin{aligned} s^{\alpha}\hat{\mathbf{U}}(\overline{\boldsymbol{\xi}}, s) - s^{\alpha-1}\mathbf{U}_0 - \mathscr{L}\hat{\mathbf{U}}(\overline{\boldsymbol{\xi}}, s) &= \hat{\mathbf{h}}(\overline{\boldsymbol{\xi}}, s), \\ \mathscr{L}_b\left\{\hat{\mathbf{U}}(\overline{\boldsymbol{\xi}}, s)\right\} &= \hat{\mathbf{g}}(\overline{\boldsymbol{\xi}}, s), \end{aligned} \tag{7}$$

which can be rearranged as

$$\left(s^{\alpha}I - \mathscr{L}\right)\left\{\hat{\mathbf{U}}(\overline{\boldsymbol{\xi}}, s)\right\} = \mathbf{U}_0 + \hat{\mathbf{h}}(\overline{\boldsymbol{\xi}}, s), \quad \overline{\boldsymbol{\xi}} \in \Omega, \tag{8}$$

$$\mathscr{L}_b\left\{\hat{\mathbf{U}}(\overline{\boldsymbol{\xi}}, s)\right\} = \hat{\mathbf{g}}(\overline{\boldsymbol{\xi}}, s), \quad \overline{\boldsymbol{\xi}} \in \partial\Omega\ , \tag{9}$$

where I denotes the identity operator, $\mathscr{L} = \Delta + \mathbf{V}(\overline{\xi}) \cdot \nabla - \mathbf{w}(\overline{\xi})I$ is the governing differential operator, and $\mathscr{L}_b$ is the boundary differential operator. In order to obtain the approximate solution of the system defined in (8) and (9), first we need to discretize the operators $\mathscr{L}$ and $\mathscr{L}_b$ via LRBFs. Afterwards, systems (8) and (9) will be solved in parallel for each point s (see, e.g., [45]). In the final step, the solution of problems (1)–(3) can be obtained by expressing it as a Bromwich integral. The next section is about the approximation of the spatial operators via the LRBF method.

3. Space Discretization via LRBF Method

Here, we propose a LRBF for approximating the three-dimensional elliptic PDEs in Laplace space. Unlike the GRBF method, the LRBF method can be employed only for small number of nodes (sub-domain) at each nodal point instead of implementing the entire set of points. This method provides a linear system that is sparse and well conditioned. Let $\Theta = \left\{\overline{\xi}_i\right\}_{i=1}^{N}$ be the set of centers in $\overline{\Omega} = \Omega \cup \partial\Omega$. For each node $\overline{\xi}_i$, we select n nearest neighbor centers $\overline{\xi}_j^{[i]}$, $j = 1, 2, \ldots, n$. The index $[i]$ denotes that the nodes belonging to the local domain Ω_i of each node $\overline{\xi}_i$. To construct the LRBFs, the collocation technique is applied to the local domain $\Omega_i = \left\{\overline{\xi}_j^{[i]}\right\}_{j=1}^{n}$, $i = 1, 2, \ldots, N$. The approximation of $\hat{\mathbf{U}}(\overline{\xi}_i, s)$ via the LRBF method is given as

$$\hat{\mathbf{U}}\left(\overline{\boldsymbol{\xi}}_i, s\right) = \sum_{j=1}^{n} \lambda_j^{[i]} \phi\left(\left\|\overline{\boldsymbol{\xi}}_i - \overline{\boldsymbol{\xi}}_j^{[i]}\right\|\right), \tag{10}$$

and by applying the collocation method in Ω_i, we have

$$\begin{pmatrix} \hat{U}\left(\overline{\boldsymbol{\xi}}_1^{[i]}, s\right) \\ \hat{\mathbf{U}}\left(\overline{\boldsymbol{\xi}}_2^{[i]}, s\right) \\ \cdot \\ \cdot \\ \cdot \\ \hat{\mathbf{U}}\left(\overline{\boldsymbol{\xi}}_n^{[i]}, s\right) \end{pmatrix} = \begin{pmatrix} \phi\left(\left\|\overline{\boldsymbol{\xi}}_1^{[i]} - \overline{\boldsymbol{\xi}}_1^{[i]}\right\|\right) & \phi\left(\left\|\overline{\boldsymbol{\xi}}_1^{[i]} - \overline{\boldsymbol{\xi}}_2^{[i]}\right\|\right) & \cdots & \phi\left(\left\|\overline{\boldsymbol{\xi}}_1^{[i]} - \overline{\boldsymbol{\xi}}_n^{[i]}\right\|\right) \\ \phi\left(\left\|\overline{\boldsymbol{\xi}}_2^{[i]} - \overline{\boldsymbol{\xi}}_1^{[i]}\right\|\right) & \phi\left(\left\|\overline{\boldsymbol{\xi}}_2^{[i]} - \overline{\boldsymbol{\xi}}_2^{[i]}\right\|\right) & \cdots & \phi\left(\left\|\overline{\boldsymbol{\xi}}_2^{[i]} - \overline{\boldsymbol{\xi}}_n^{[i]}\right\|\right) \\ \cdot & \cdot & \cdots & \cdot \\ \cdot & \cdot & \cdots & \cdot \\ \cdot & \cdot & \cdots & \cdot \\ \phi\left(\left\|\overline{\boldsymbol{\xi}}_n^{[i]} - \overline{\boldsymbol{\xi}}_1^{[i]}\right\|\right) & \phi\left(\left\|\overline{\boldsymbol{\xi}}_n^{[i]} - \overline{\boldsymbol{\xi}}_2^{[i]}\right\|\right) & \cdots & \phi\left(\left\|\overline{\boldsymbol{\xi}}_n^{[i]} - \overline{\boldsymbol{\xi}}_n^{[i]}\right\|\right) \end{pmatrix} \begin{pmatrix} \lambda_1^{[i]} \\ \lambda_2^{[i]} \\ \cdot \\ \cdot \\ \cdot \\ \lambda_n^{[i]} \end{pmatrix}. \tag{11}$$

Denote the matrix in equation (11) by $\mathbf{G}^{[i]}$, where $\phi(\|\bar{\xi}_i - \bar{\xi}_j^{[i]}\|)$ is a radial kernel, $\|.\|$ is the Euclidean norm, and $\{\lambda_j^{[i]}\}_{j=1}^{N}$ are the unknown coefficients. There are a large number of RBFs which are used commonly including the Gaussian (GA), multiquadrics (MQ), thin-plate splines (TPS), and inverse multiquadrics (IMQ). Among these RBFs, the multiquadric (MQ) is perhaps the most popular that is used in applications [41]; therefore, in this study, we have selected the MQ, which is given as

$$\phi\left(\left\|\bar{\xi}_i - \bar{\xi}_j^{[i]}\right\|\right) = \sqrt{1 + \left(\mathbf{S_p}\left\|\bar{\xi}_i - \bar{\xi}_j^{[i]}\right\|\right)^2}, \tag{12}$$

where $\mathbf{S_p}$ denotes the shape parameter. Each node $\bar{\xi}_i$ and its n nearest neighbor points are called stencils [43]. A typical stencil for $n = 7$ is shown in Figure 1.

At each stencil, we obtain an $n \times n$ matrix of the form

$$\hat{\mathbf{U}}^{[i]} = \mathbf{G}^{[i]}\boldsymbol{\lambda}^{[i]}, \quad i = 1, 2, \ldots, N, \tag{13}$$

where $\hat{\mathbf{U}}^{[i]} = [\hat{\mathbf{U}}(\bar{\xi}_1^{[i]}), \hat{\mathbf{U}}(\bar{\xi}_2^{[i]}), \ldots, \hat{\mathbf{U}}(\bar{\xi}_n^{[i]})]^T$ and $\lambda^{[i]} = [\lambda_1^{[i]}, \lambda_2^{[i]}, \ldots, \lambda_n^{[i]}]^T$. In [46], the invertibility of the system matrix $\mathbf{G}^{[i]}$ based on strictly positive definite kernel functions for distinct nodes was proved. The coefficients $\lambda^{[i]}$ in (13) can be obtained as

$$\boldsymbol{\lambda}^{[i]} = \left(\mathbf{G}^{[i]}\right)^{-1}\hat{\mathbf{U}}^{[i]}, \quad \text{for } i = 1, 2, \ldots, N. \tag{14}$$

The next step in the LRBF scheme is as follows:

$$\mathscr{L}\hat{\mathbf{U}}\left(\bar{\xi}_i\right) = \sum_{j=1}^{n} \boldsymbol{\lambda}_j^{[i]} \mathscr{L}\phi\left(\left\|\bar{\xi}_i - \bar{\xi}_j^{[i]}\right\|\right), \tag{15}$$

and from the above equation, we can write

$$\begin{aligned} \mathscr{L}\hat{\mathbf{U}}\left(\bar{\xi}_i\right) &= \boldsymbol{\lambda}^{[i]} \cdot \Upsilon^{[i]} \\ &= \Upsilon^{[i]} \cdot \boldsymbol{\lambda}^{[i]} \\ &= \Upsilon^{[i]}\left(\mathbf{W}^{[\mathbf{i}]}\right)^{-1}\hat{\mathbf{U}}^{[i]}. \end{aligned} \tag{16}$$

Hence, we have

$$\mathscr{L}\hat{\mathbf{U}}\left(\bar{\xi}_i\right) = \boldsymbol{\Psi}^{[i]}\hat{\mathbf{u}}^{[i]}, \tag{17}$$

where $\Psi^{[i]} = \Upsilon^{[i]}(\mathbf{W}^{[\mathbf{i}]})^{-1}$ and $\Upsilon^{[i]} = \mathscr{L}\phi(\|\bar{\xi}_i - \bar{\xi}_j^{[i]}\|)$ is a $1 \times n$ vector. Equation (17) gives us the local form, and the global form can be obtained by expanding the matrix $\Psi^{[i]}$ to Ψ by adding zeros to corresponding position in each row [41]. Thus, the differential operator $\mathscr{L}$ is approximated at each center $\bar{\xi}_i$ via the LRBF method as

$$\mathscr{L}\hat{\mathbf{U}} \equiv \boldsymbol{\Psi}\hat{\mathbf{u}}. \tag{18}$$

The matrix $\Psi_{N\times N}$ is sparse with n non-zero entries and $N - n$ zero entries. We can similarly approximate the operator $\mathscr{L}_b$ as

$$\mathscr{L}_b\hat{\mathbf{U}} \equiv \Xi\hat{\mathbf{u}}, \tag{19}$$

and substituting equations (18) and (19) in equations (8) and (9), we get

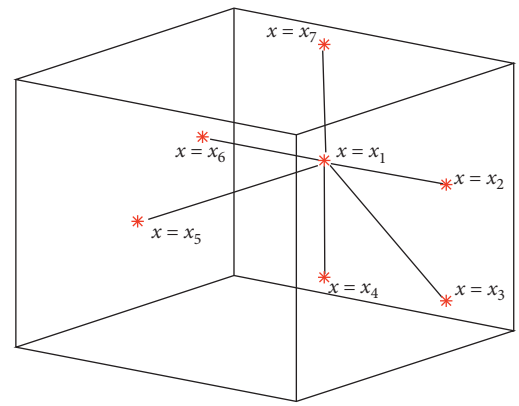

Figure 1: A typical stencil for $n = 7$.

$$\left(s^{\alpha}I - \boldsymbol{\Psi}\right)\left\{\hat{\mathbf{U}}(\bar{\xi}, s)\right\} = u_0 + \hat{h}(\bar{\xi}, s), \quad \bar{\xi} \in \Omega, \tag{20}$$

$$\Xi\left\{\hat{\mathbf{U}}(\bar{\xi}, s)\right\} = \hat{g}(\bar{\xi}, s), \quad \bar{\xi} \in \partial\Omega\,. \tag{21}$$

Solving the above system defined in equations (20) and (21) for each point s, we will obtain the approximate solution $\hat{\mathbf{U}}(\bar{\xi}, s)$.

3.1. Algorithm for Optimal Shape Parameter. The MQ kernel function defined in (12) includes a parameter $\mathbf{S_p}$ which can be varied on every local domain to enhance the accuracy of numerical solution. To estimate the accuracy of approximate solution and quantify the sensitivity to perturbation of the linear system, the condition number (C_N) of the interpolation matrix $\mathbf{G}^{[i]}$ may be used. We utilized the uncertainty principle [47] for a decent estimation of the shape parameter $\mathbf{S_p}$. In RBF methods for ill-conditioned matrices, better accuracy is achieved. Using the uncertainty principle, when (C_N) is kept approximately in the range $10^{12} < C_N < 10^{16}$, smallest error occurs. The matrix $\mathbf{G}^{[i]}$ can be expressed as $\mathbf{Q}, \mathbf{S}, \mathbf{V} = sv\,d(\mathbf{G}^{[i]})$, where $\mathbf{S}_{n\times n}$ is diagonal matrix which contains the singular values of $\mathbf{G}^{[i]}$. $\mathbf{Q}_{n\times n}$, $\mathbf{V}_{n\times n}$ are orthogonal matrices, and the condition number C_N can be computed as $C_N = \|\mathbf{G}^{[i]}\|\|(\mathbf{G}^{[i]})^{-1}\| = \max(\mathbf{S})/\min(\mathbf{S})$.

The following algorithm in MATLAB can be used to search for optimal shape parameter (Algorithm 1).

After getting an optimal shape parameter $\mathbf{S_p}$, the svd is used to compute $(\mathbf{G}^{[i]})^{-1} = (QSV^T)^{-1} = VS^{-1}Q^T$ (see [48]). Hence, the weights $\Psi^{[i]}$ in (18) can be computed.

4. Stability

For the stability of systems (20) and (21), we write the system as

$$\mathbf{A}\hat{\mathbf{U}}(\bar{\xi}, s) = \mathbf{b}. \tag{22}$$

$\mathbf{A}_{N\times N}$ is sparsely obtained via the LRBF method. We define a constant for the aforementioned system as

$$Q = \sup_{\hat{\mathbf{U}}\neq 0} \frac{\|\hat{\mathbf{U}}(\bar{\xi}, s)\|}{\|\mathbf{A}\hat{\mathbf{U}}(\bar{\xi}, s)\|}, \tag{23}$$

Step 1: set $C_N = 1$
Step 2: select $10^{12} < C_N < 10^{16}$
Step 3: while $C_N > C_{N\,\text{maximum}}$ and $C_N < C_{N\,\text{minimum}}$
Step 4: $\mathbf{Q}, \mathbf{S}, \mathbf{V} = sv\ d(\mathbf{G}^{[i]})$
Step 5: $C_N = (\max(\mathbf{S})/\min(\mathbf{S}))$
Step 6: if $C_N < C_{N\,\text{minimum}}$, $\mathbf{S_p} = \mathbf{S_p} - \mathbf{S_p}$ Increament
Step 7: else $C_N > C_{N\,\text{maximum}}$, $\mathbf{S_p} = \mathbf{S_p} + \mathbf{S_p}$ Increament
return $\mathbf{S_p}$.

Algorithm 1: Algorithm for optimal shape parameter.

called the constant of stability. Also, using norm $\|.\|$ on $R^N Q$ is finite. From (23), we have

$$\|\mathbf{A}\|^{-1} \leq \frac{\|\hat{\mathbf{U}}(\bar{\boldsymbol{\xi}}, s)\|}{\|\mathbf{A}\hat{\mathbf{U}}(\bar{\boldsymbol{\xi}}, s)\|} \leq Q. \tag{24}$$

Similarly, we have

$$\left\|\mathbf{A}^{\dagger}\right\| = \sup_{v \neq 0} \frac{\left\|\mathbf{A}^{\dagger} v\right\|}{\|v\|}, \tag{25}$$

where $\mathbf{A}^{\dagger}$ is the pseudoinverse of $\mathbf{A}$, and thus we have

$$\left\|\mathbf{A}^{\dagger}\right\| \geq \sup_{v=\mathbf{A}\hat{\mathbf{U}}\neq 0} \frac{\left\|\mathbf{A}^{\dagger}\mathbf{A}\hat{\mathbf{U}}(\bar{\boldsymbol{\xi}}, s)\right\|}{\|\mathbf{A}\hat{\mathbf{U}}(\bar{\boldsymbol{\xi}}, s)\|} = \sup_{\hat{\mathbf{U}}\neq 0} \frac{\|\hat{\mathbf{U}}(\bar{\boldsymbol{\xi}}, s)\|}{\|\mathbf{A}\hat{\mathbf{U}}(\bar{\boldsymbol{\xi}}, s)\|} = Q. \tag{26}$$

Equations (24) and (26) confirm the bounds for Q. The calculation of the pseudoinverse for the approximation of the system defined in (22) may be hard computationally, but it validates the stability. The MATLAB function condest provides the estimation for $\|\mathbf{A}^{-1}\|_{\infty}$, and thus

$$Q = \frac{\text{condest}(A')}{\|\mathbf{A}\|_{\infty}}. \tag{27}$$

5. Numerical Inversion of Laplace Transform

After solving the system defined in (20) and (21) for each node s, we obtain the solution of (1)–(3) via the inversion of Laplace transformation as

$$\mathbf{U}(\bar{\boldsymbol{\xi}}, \tau) = \frac{1}{2\pi i} \int_{\sigma - i\infty}^{\sigma + i\infty} e^{s\tau} \hat{\mathbf{U}}(\bar{\boldsymbol{\xi}}, s) \mathrm{d}s. \tag{28}$$

In applying the LT method, the main hurdle is the inversion of the LT. In most of the cases, it is quite difficult to invert the LT analytically. Therefore, we need some numerical techniques for the inversion of LT. In the literature, a large number of techniques are available for the inversion of LT [49], among which one of the efficient and easy methods in implementation is the method of contour integration used in combination with trapezoidal and midpoint rules. To handle the exponential factor in equation (28), contour deformation is performed. Particularly, the contour in equation (28) can be deformed to a Hankel contour [50]. The exponential factors on these contours decay rapidly making the integral in equation (28) appropriate for solving via trapezoidal or midpoint rule [50–52]. In this work, we consider a contour having the following parametric form:

$$\Lambda\colon\ s = s(\boldsymbol{\beta}), \quad -\pi \leq \boldsymbol{\beta} \leq \pi, \tag{29}$$

where $\mathrm{Res}(\pm\pi) = -\infty$, and

$$s(\boldsymbol{\beta}) = \frac{M\vartheta(\boldsymbol{\beta})}{t}, \tag{30}$$

where

$$\vartheta(\boldsymbol{\beta}) = -\boldsymbol{\varrho} + \boldsymbol{\xi}\boldsymbol{\beta}\cot(\boldsymbol{\rho}\boldsymbol{\beta}) + \boldsymbol{\zeta}\imath\boldsymbol{\beta}, \tag{31}$$

and the parameters $\boldsymbol{\varrho}$, ρ, ξ, and ζ must be selected by the user. From equations (28) and (30), we get

$$\begin{aligned}\mathbf{U}(\bar{\boldsymbol{\xi}}, \tau) &= \frac{1}{2\pi i} \int_{\Lambda} e^{s\tau} \hat{U}(\bar{\boldsymbol{\xi}}, s) \mathrm{d}s \\ &= \frac{1}{2\pi i} \int_{-\pi}^{\pi} e^{s(\boldsymbol{\beta})\tau} \hat{\mathbf{U}}(\bar{\boldsymbol{\xi}}, s(\boldsymbol{\beta})) s'(\boldsymbol{\beta}) \mathrm{d}\boldsymbol{\beta}.\end{aligned} \tag{32}$$

The M-panel midpoint rule with $k = (2\pi/M)$ is used to evaluate the integral in equation (32) numerically as

$$\begin{aligned}&\mathbf{U}_k(\bar{\boldsymbol{\xi}}, \tau) = \frac{1}{Mi} \sum_{j=1}^{M} e^{s_j\tau} \hat{\mathbf{U}}\left(\bar{\boldsymbol{\xi}}, s_j\right) s_j', \\ &\text{for } s_j = s\left(\boldsymbol{\beta}_j\right), s_j' = s'\left(\boldsymbol{\beta}_j\right) \text{ and } \boldsymbol{\beta}_j = -\pi + \left(j - \frac{1}{2}\right)k.\end{aligned} \tag{33}$$

5.1. Convergence and Accuracy. While obtaining the numerical solution of problems (1)–(3), we utilized the LT in combination with the LRBF method. First we apply the LT to reduce the problem to an equivalent elliptic PDE, and no error occurs in this step. In the second step, we employ the LRBF for approximating the solution of the elliptic PDE. The error estimate of the LRBF method is of order $O(\mu^{(1/\mathbf{S_p}h)})$, $0 < \mu < 1$, where h and $\mathbf{S_p}$ are the fill distance and the shape parameter, respectively [53]. While solving the integral in equation (32) numerically, the convergence of the quadrature rule is achieved at different time rates which rely on the step size k, the domain $[t_0, T]$, and the path Λ. The error analysis of improved Talbot's method is based on the following theorem.

Theorem 1 (see [50]). *Let β_j be defined as in (33). If $f: D \longrightarrow \mathbb{C}$ is an analytic function in the set*

$$D = \{\beta \in \mathbb{C}: \ -\pi < \mathrm{Re}\beta < \pi \text{ and } -d < \mathrm{Im}\beta < c\}, \tag{34}$$

when $c, d > 0$, then

$$\int_{-\pi}^{\pi} f(\beta)\mathrm{d}\beta - \frac{2\pi}{M}\sum_{j=1}^{M} f\left(\beta_j\right) = B_-(\theta) + B_+(\vartheta), \tag{35}$$

where

$$\begin{aligned} B_+(\vartheta) &= \frac{1}{2}\left(\int_{-\pi}^{-\pi+\iota\vartheta} + \int_{-\pi+\iota\vartheta}^{\pi+\iota\vartheta} + \int_{\pi+\iota\vartheta}^{\pi}\right)\left(1 + \iota\tan\left(\frac{M\beta}{2}\right)\right) f(\beta)\mathrm{d}\beta, \\ B_-(\theta) &= \frac{1}{2}\left(\int_{-\pi}^{-\pi-\iota\vartheta} + \int_{-\pi-\iota\vartheta}^{\pi-\iota\vartheta} + \int_{\pi-\iota\vartheta}^{\pi}\right)\left(1 - \iota\tan\left(\frac{M\beta}{2}\right)\right) f(\beta)\mathrm{d}\beta, \end{aligned} \tag{36}$$

$\forall 0 < \vartheta < c$ and $0 < \theta < d$ and M even; for odd M, we can replace $\tan(M\beta/2)$ with $-\cot(M\beta/2)$, and if $f(\beta)$ is real valued, that is, $f(\overline{\beta}) = \overline{f(\beta)}$, then

$$B(\vartheta) = B_+(\vartheta) + B_-(\vartheta) = \mathrm{Re}\int_{-\pi+\iota\vartheta}^{\pi+\iota\vartheta}\left(1 + \iota\tan\left(\frac{M\beta}{2}\right)\right) f(\beta)\mathrm{d}\beta, \tag{37}$$

and by analyzing the behavior of tangent function in complex, this can be bounded as

$$|B(\vartheta)| \le \frac{4\pi\mathscr{C}}{\exp(cM) - 1}, \tag{38}$$

where M is assumed to be even and $\mathscr{C}$ and c are some positive constants. For odd M, the analysis is similar.

For optimal accuracy, one needs optimal parameters in equation (30). The authors [50] have obtained the optimal parameters given as

ξ	0.50170
ϱ	0.61220
ζ	0.26450
ρ	0.64070

with the error estimate

$$\mathrm{error}_{\mathrm{est}} = \left|\mathbf{U}(\overline{\boldsymbol{\xi}}, t) - \mathbf{U}_k(\overline{\boldsymbol{\xi}}, t)\right| = O\left(e^{-1.3580M}\right). \tag{39}$$

6. Numerical Experiments

To check the performance of the proposed transformed LRBF method, we have used three error measures. They are the absolute error Error 1, the maximum absolute error Error 2, and the relative error Error 3 which are defined as follows:

$$\begin{aligned} \text{Error 1} &= \left|\mathbf{U}\left(\overline{\boldsymbol{\xi}}_i\right) - \mathbf{U}_k\left(\overline{\boldsymbol{\xi}}_i\right)\right|, \\ \text{Error 2} &= \max\left(\mathrm{error}_{\mathrm{abs}}\right), \\ \text{Error 3} &= \sqrt{\frac{\sum_{i=1}^{N}\left(\mathbf{U}\left(\overline{\boldsymbol{\xi}}_i\right) - \mathbf{U}_k\left(\overline{\boldsymbol{\xi}}_i\right)\right)^2}{\sum_{i=1}^{N}\left(\mathbf{U}\left(\overline{\boldsymbol{\xi}}_i\right)\right)^2}}, \end{aligned} \tag{40}$$

where $\mathbf{U}(\overline{\xi}, \tau)$ and $\mathbf{U}_k(\overline{\xi}, \tau)$ are the analytical and numerical solutions, respectively. We test our proposed method using two examples.

6.1. Problem 1. Consider equation (1) with exact solution as [54]

$$\mathbf{U}(x, y, z, t) = e^{(\gamma_1 t - \gamma_2 x + \gamma_2 y + \gamma_2 z)}, \quad \Omega = [-1, 1]^3, t > 0, \tag{41}$$

where $\gamma_2 = \sqrt{(\gamma_1/6)}$, $\gamma_1 = 0.1$, $\mathbf{V}(\xi) = (-\gamma_2, -\gamma_2, -\gamma_2)^T$, $\mathbf{w}(\xi) = 0$, and $\mathbf{h}(\overline{\xi}, t) = 0$. The accuracy of the problem is investigated at $t = 1$ in cube domain $[-1, 1]^3$ with $\alpha = 0.1, 0.5, 0.9$. Table 1 shows the maximum absolute error Error 2 and relative error Error 3 for several nodes N, stencil size $n = 80$, and $M = 28$. Table 2 shows the maximum absolute error Error 2 and relative error Error 3 for several stencil sizes n, $N = 1728$, and $M = 26$. It is clear that the method has approximated the problem with acceptable accuracy. We observe that the proposed method produced accurate results. The numerical solution in rectangular area with different values of α is given in Figures 2(a)–2(c). In Figures 3(a) and 3(b), the exact and numerical solutions in the xz-plane for $y = -1, -0.5, 0, 0.5, 1$ are shown; it is observed that the exact and numerical solutions are in better agreement. Figures 4(a)–4(c) show the plots of absolute errors for different values of the fractional order α with $N = 3375$, $n = 81$, and $M = 26$. From the figures, we see that the method has produced accurate results. In Figures 5(a)–5(c), the contour slice plots of the absolute errors for various values of α in rectangular area using $N = 3375$, $n = 81$, and $M = 26$ are presented. We also plot the contour graphs of absolute error for various values of α with $N = 3375$, $n = 81$, $M = 26$, and $z = 0.5$ in Figures 6(a)–6(c). Also, the graph of absolute error for $\alpha = 0.9$ with $N = 225$, $n = 81$, $M = 26$, and $y = -0.5$ is shown in Figure 7(a) and that for $\alpha = 0.95$ with $N = 400$, $n = 25$, $M = 26$, and $y = -0.5$ is shown Figure 7(b). A high accuracy is observed.

6.2. Problem 2. Consider equation (1) with exact solution given as [55]

Table 1: The computational results for problem 1 with N in the domain $[-1,1]^3$.

$n = 80, M = 28$	$N \longrightarrow$	125	216	729	1728	3375
$\alpha = 0.1$	Error 2	8.00×10^{-3}	3.89×10^{-4}	4.38×10^{-4}	4.49×10^{-4}	4.88×10^{-4}
	Error 3	1.60×10^{-3}	1.21×10^{-4}	1.30×10^{-4}	1.40×10^{-4}	1.55×10^{-4}
$\alpha = 0.5$	Error 2	8.00×10^{-3}	1.00×10^{-3}	1.10×10^{-3}	1.10×10^{-3}	1.00×10^{-3}
	Error 3	1.80×10^{-3}	3.47×10^{-4}	4.08×10^{-4}	4.32×10^{-4}	4.36×10^{-4}
$\alpha = 0.9$	Error 2	8.00×10^{-3}	5.78×10^{-4}	6.02×10^{-4}	5.97×10^{-4}	5.61×10^{-4}
	Error 3	1.80×10^{-3}	1.92×10^{-4}	2.23×10^{-4}	2.35×10^{-4}	2.31×10^{-4}

Table 2: The computational results for problem 1 with N in the domain $[-1,1]^3$.

$M = 26, N = 1728$	$n \longrightarrow$	40	50	60	83	85
$\alpha = 0.1$	Error 2	1.20×10^{-3}	1.50×10^{-3}	4.60×10^{-3}	4.48×10^{-4}	7.15×10^{-4}
	Error 3	2.00×10^{-4}	1.81×10^{-4}	4.55×10^{-4}	1.40×10^{-4}	5.87×10^{-4}
$\alpha = 0.5$	Error 2	1.60×10^{-3}	1.50×10^{-3}	4.60×10^{-3}	1.10×10^{-3}	7.00×10^{-4}
	Error 3	4.58×10^{-4}	4.58×10^{-4}	5.75×10^{-4}	4.32×10^{-4}	5.74×10^{-4}
$\alpha = 0.9$	Error 2	1.40×10^{-3}	1.40×10^{-3}	4.60×10^{-3}	5.97×10^{-4}	5.97×10^{-4}
	Error 3	2.78×10^{-4}	2.73×10^{-4}	4.64×10^{-4}	2.35×10^{-4}	5.50×10^{-4}

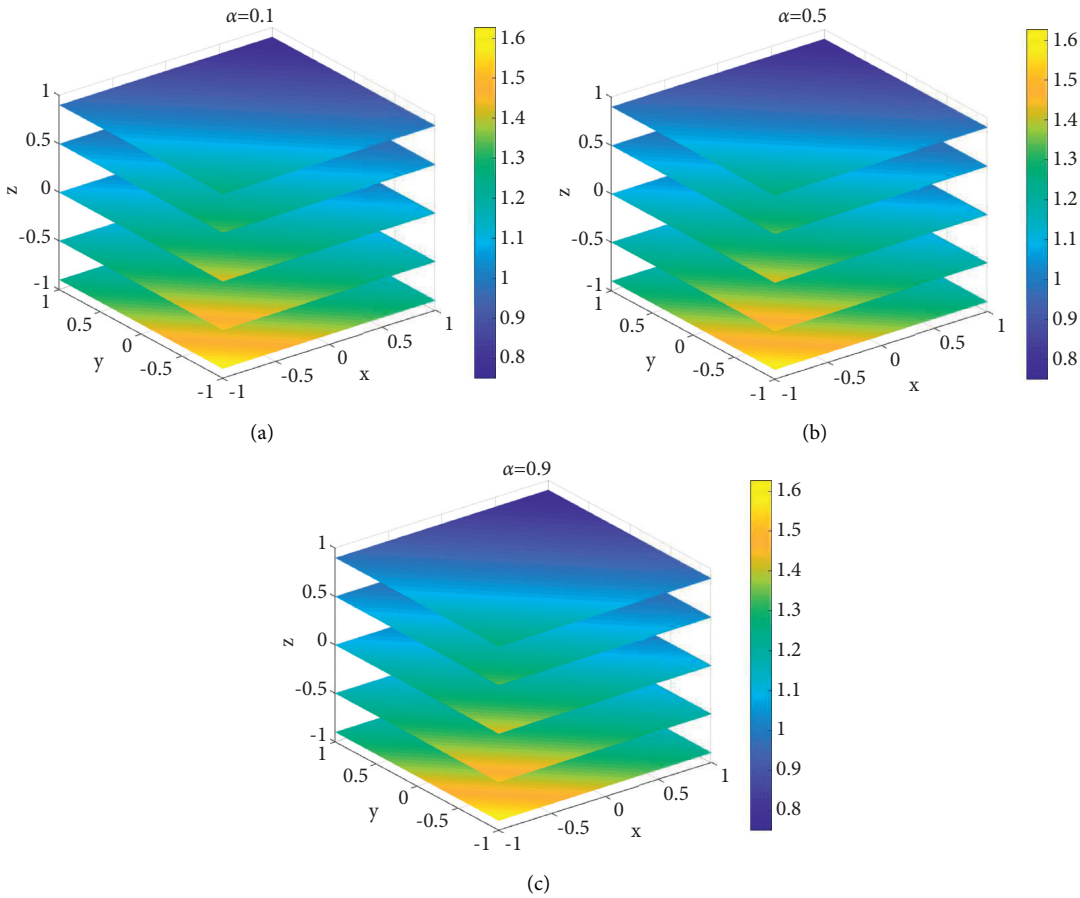

Figure 2: Approximate solution in rectangular area using various values of α with $N = 1728$, $n = 40$, and $M = 26$.

$$\mathbf{U}(x,y,z,t) = t^{(\alpha+3)}\sin(\pi x)\sin(\pi y)\sin(\pi z), \quad t>0, \tag{42}$$

with $\mathbf{w}(\xi) = 1, \mathbf{V}(\xi) = (1,1,1)^T$ and the forcing term $\mathbf{h}(\overline{\xi},t)$ is specified to satisfy the given equation and the exact solution. The initial and boundary data are extracted from the exact solution. The accuracy of the problem is investigated in cube domain $[0,1]^3$ at $t = 1$ for $\alpha = 0.1, 0.5, 0.9$. Table 3 shows the maximum absolute error Error 2 and relative error Error 3 for several nodes N, stencil size $n = 80$, and $M = 28$. Table 4 shows the maximum absolute error Error 2 and relative error Error 3 for several values of M, $N = 4913$, and stencil size

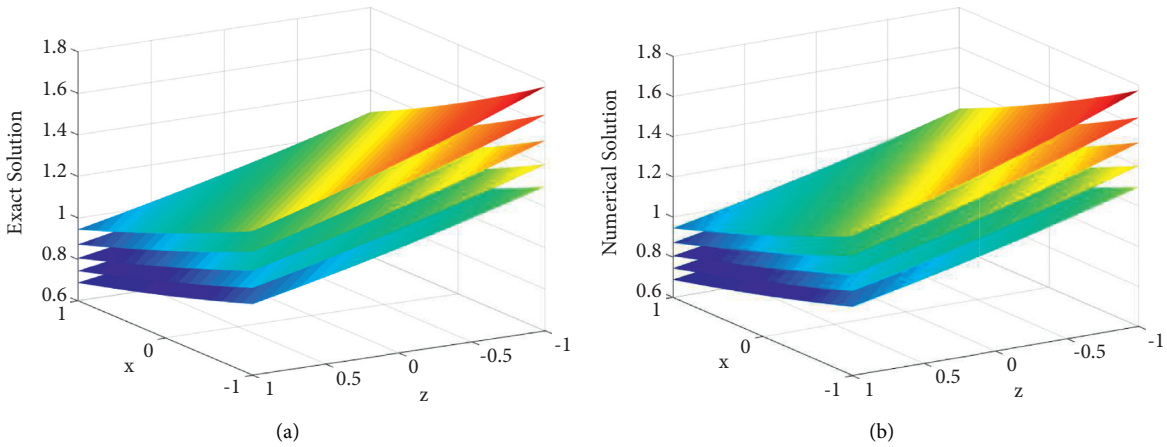

Figure 3: Exact and numerical solutions of problem 1 with $\alpha = 0.1$ and $y = -1, -0.5, 0, 0.5, 1$.

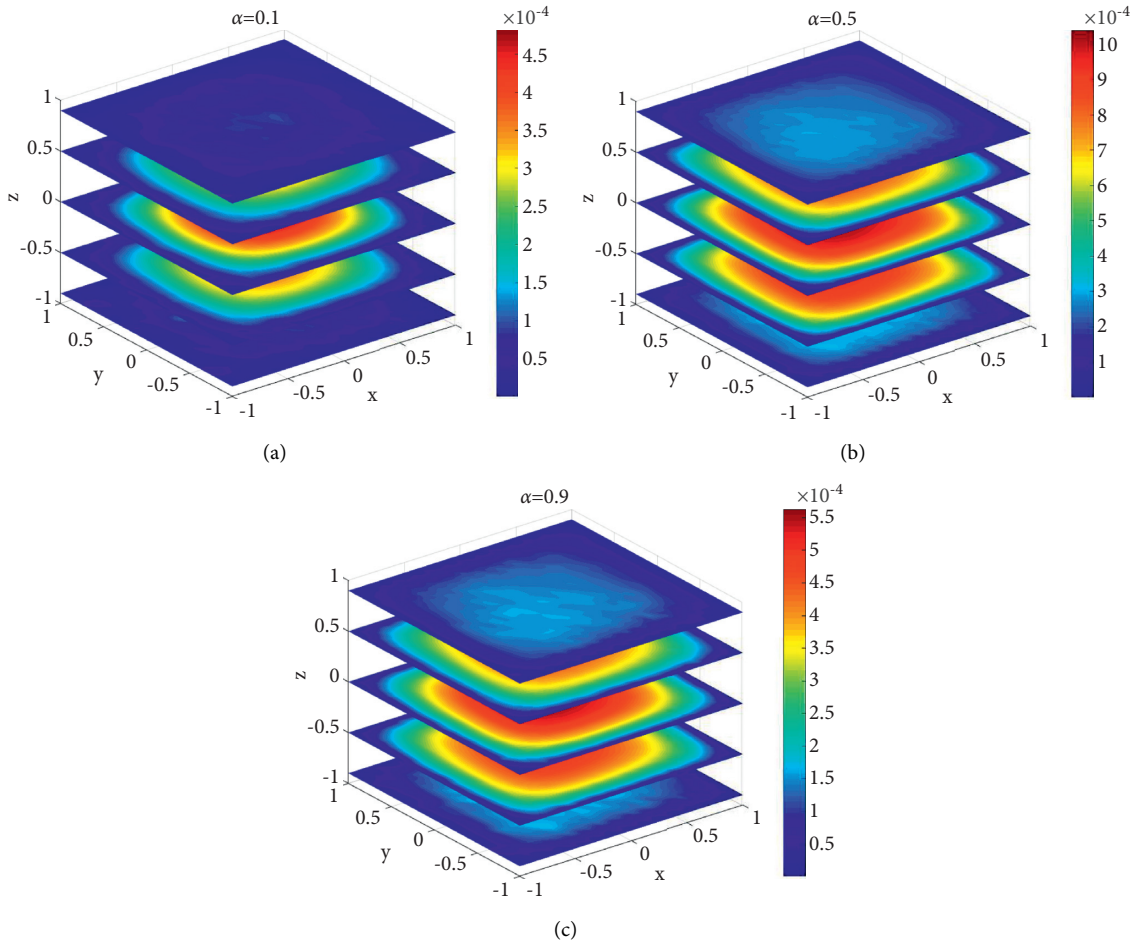

Figure 4: Absolute error in rectangular area using different values of α with $N = 3375$, $n = 81$, and $M = 26$.

$n = 83$. The numerical solutions in rectangular area for different values of α are presented in Figures 8(a)–8(c). The slice plots of exact and numerical solutions using $\alpha = 0.85$, $N = 2744$, $n = 85$, and $M = 26$ are shown in Figures 9(a) and 9(b). Exact and numerical solutions with $\alpha = 0.1$, $N = 4096$, $n = 85$, $M = 28$, and $z = 0.4, 0.6, 0.8$ are shown in Figures 10(a) and 10(b), respectively. Absolute error in rectangular area using various values of α with $N = 1000$, $n = 75$, and $M = 28$ is presented in Figures 11(a)–11(c). The contour slice plots of absolute error in rectangular area using various values of α with $N = 4096$, $n = 85$, and $M = 28$ are shown in Figures 12(a)–12(c). The contour graphs of absolute error

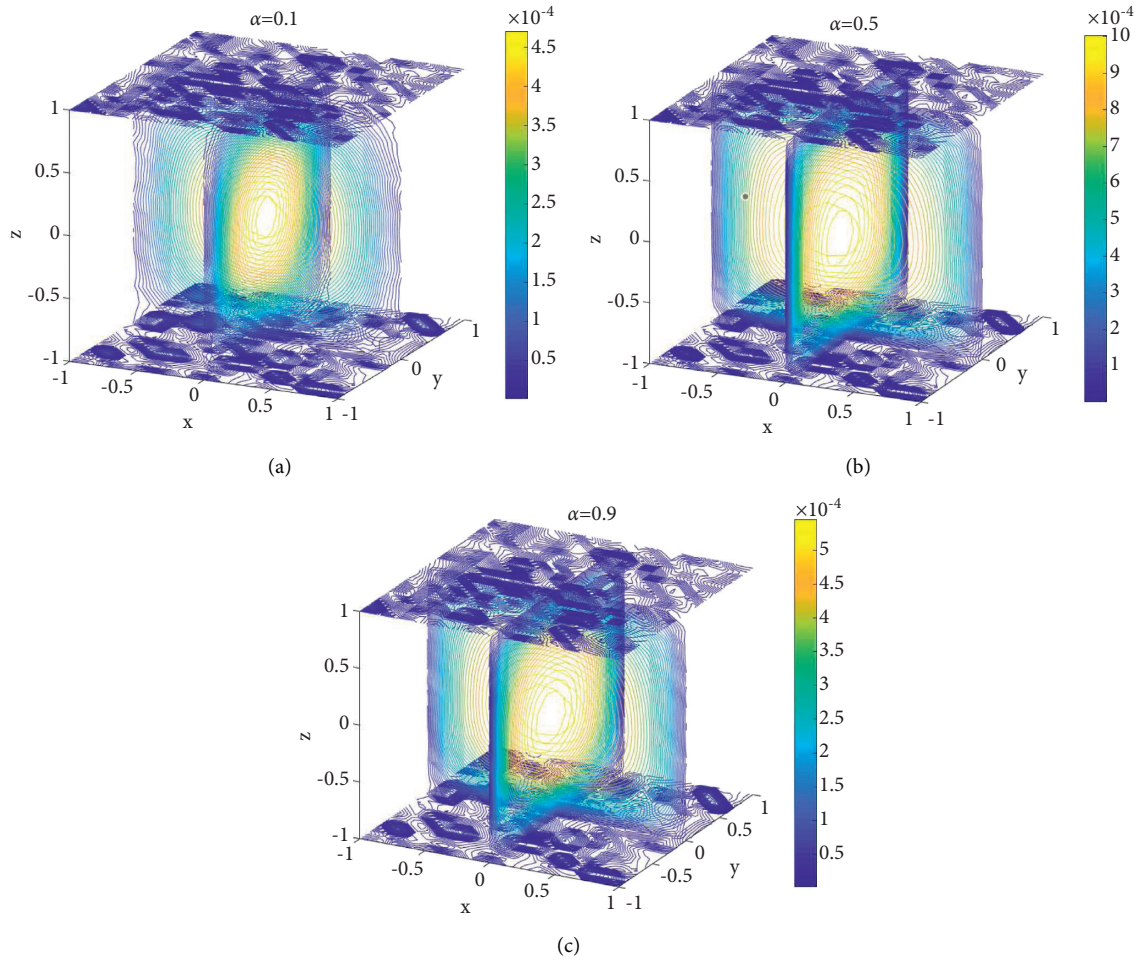

Figure 5: Contour slice of absolute error in rectangular area using different values of α with $N = 3375$, $n = 81$, and $M = 26$.

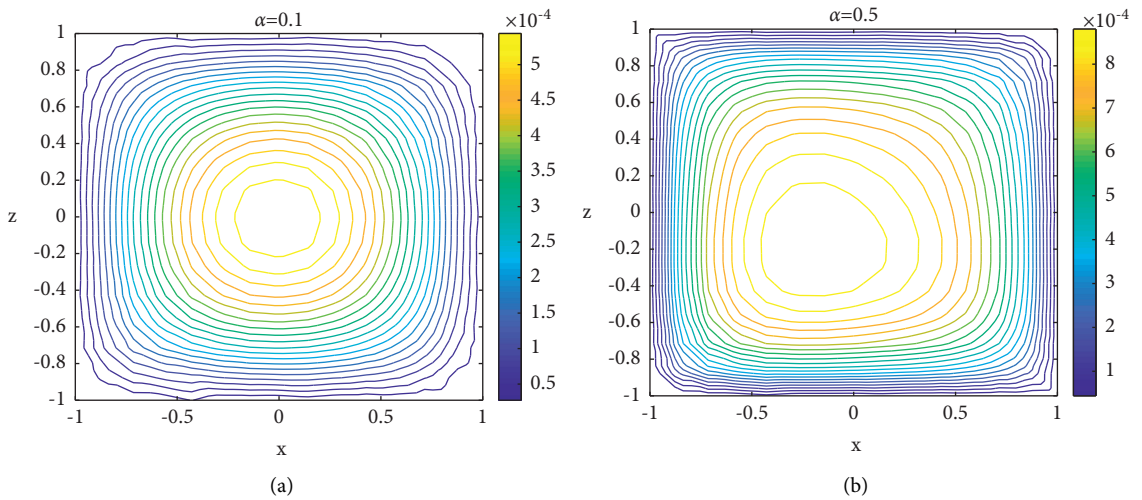

Figure 6: Continued.

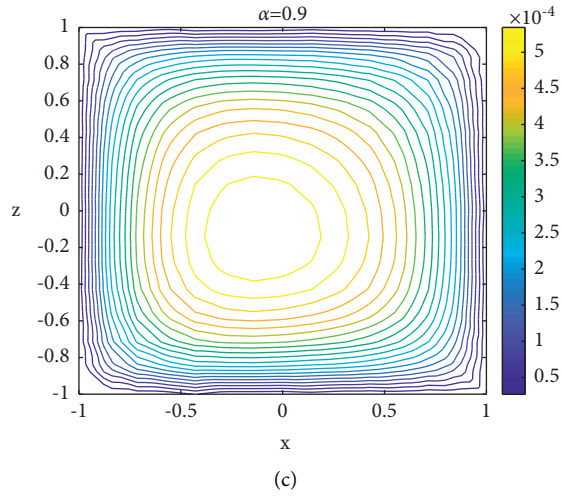

Figure 6: Contour plots of absolute error in rectangular area using different values of α with $N = 225$, $n = 81, M = 26$, and $y = 0.5$.

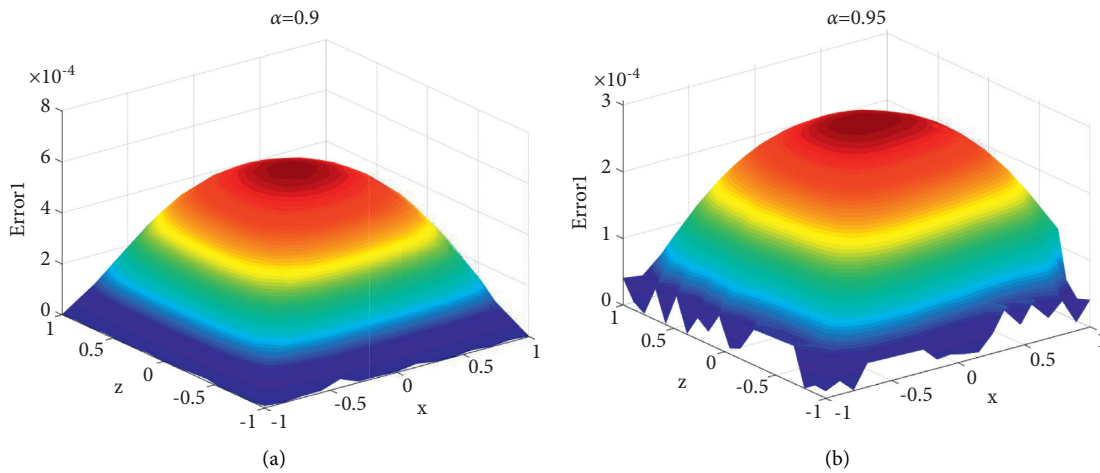

Figure 7: (a) Plot of absolute error with $\alpha = 0.9$, $N = 225$, $n = 81, M = 26$, and $y = -0.5$. (b) Plot of absolute error with $\alpha = 0.95$, $N = 400$, $n = 25, M = 26$, and $y = -0.5$.

Table 3: The computational results for problem 1 with N in the domain $[0, 1]^3$.

$n = 80, M = 28$	$N \longrightarrow$	125	216	729	1728	3375
$\alpha = 0.1$	Error 2	1.90×10^{-3}	8.07×10^{-4}	6.66×10^{-4}	7.23×10^{-4}	8.39×10^{-4}
	Error 3	3.20×10^{-3}	7.92×10^{-4}	7.89×10^{-4}	5.38×10^{-4}	6.61×10^{-4}
$\alpha = 0.5$	Error 2	1.90×10^{-3}	7.98×10^{-4}	6.60×10^{-4}	7.11×10^{-4}	8.22×10^{-4}
	Error 3	3.10×10^{-3}	7.85×10^{-4}	7.81×10^{-4}	5.31×10^{-4}	6.47×10^{-4}
$\alpha = 0.9$	Error 2	1.80×10^{-3}	7.82×10^{-4}	6.48×10^{-4}	6.90×10^{-4}	7.92×10^{-4}
	Error 3	3.00×10^{-3}	7.71×10^{-4}	7.65×10^{-4}	5.19×10^{-4}	6.22×10^{-4}
[55]	—	—	—	—	2.35×10^{-3}	—

Table 4: The computational results for problem 1 with N in the domain $[0, 1]^3$.

$n = 83, N = 4913$	$M \longrightarrow$	20	22	24	26	28
$\alpha = 0.1$	Error 2	7.14×10^{-4}	7.14×10^{-4}	7.15×10^{-4}	7.15×10^{-4}	7.15×10^{-4}
	Error 3	5.86×10^{-4}	5.87×10^{-4}	5.87×10^{-4}	5.87×10^{-4}	5.87×10^{-4}
$\alpha = 0.5$	Error 2	6.98×10^{-4}	6.99×10^{-4}	7.00×10^{-4}	7.00×10^{-4}	7.00×10^{-4}
	Error 3	5.72×10^{-4}	5.74×10^{-4}	5.74×10^{-4}	5.74×10^{-4}	5.74×10^{-4}
$\alpha = 0.9$	Error 2	6.66×10^{-4}	6.72×10^{-4}	6.72×10^{-4}	6.72×10^{-4}	6.72×10^{-4}
	Error 3	5.44×10^{-4}	5.49×10^{-4}	5.50×10^{-4}	5.50×10^{-4}	5.50×10^{-4}
[55]	—	—	—	—	2.35×10^{-3}	—

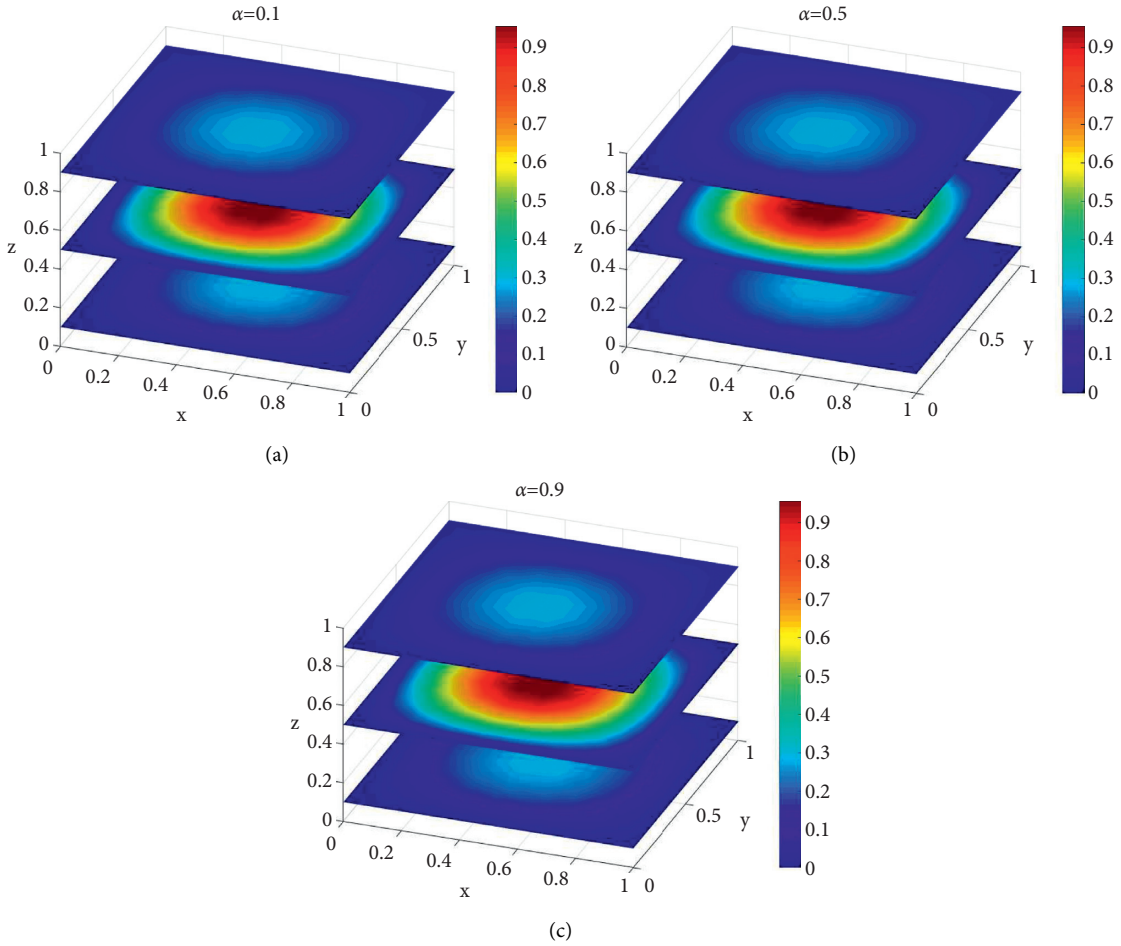

Figure 8: Approximate solution in rectangular area using different values of α with $N = 1000$, $n = 75$, and $M = 28$.

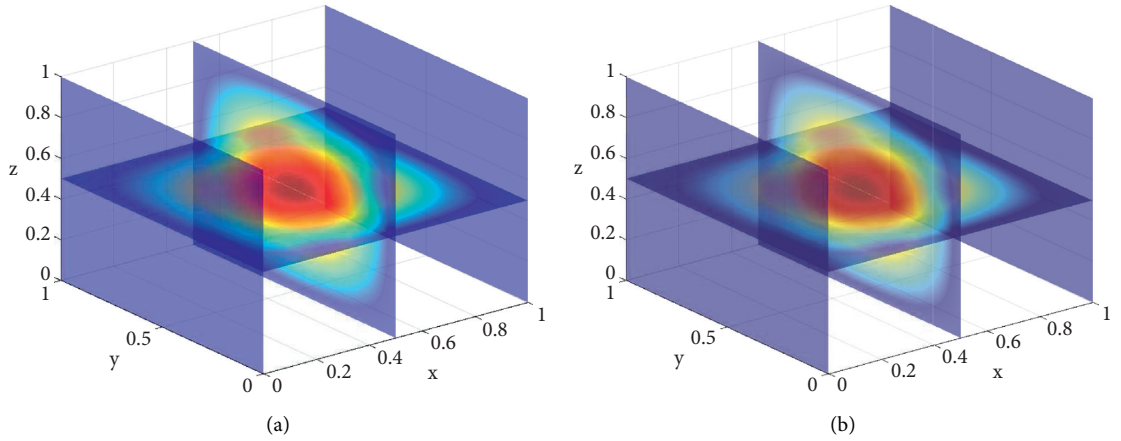

Figure 9: Slice plots of exact and approximate solutions of problem 2 with $\alpha = 0.85, N = 2744, n = 85$, and $M = 26$.

using various values of α with $N = 4096, n = 85, M = 28$, and $z = 0.5$ are presented shown in Figures 13(a)–13(c). Also, the graph of absolute error for $\alpha = 0.9$ with $N = 256, n = 25, M = 28$, and $z = 0.2$ is shown in Figure 14(a) and that for $\alpha = 0.95$ with $N = 625, n = 38, M = 28$, and $z = 0.8$ is shown Figure 14(b). From all the obtained results presented in figures and tables, we conclude that the proposed method is stable, accurate, and efficient.

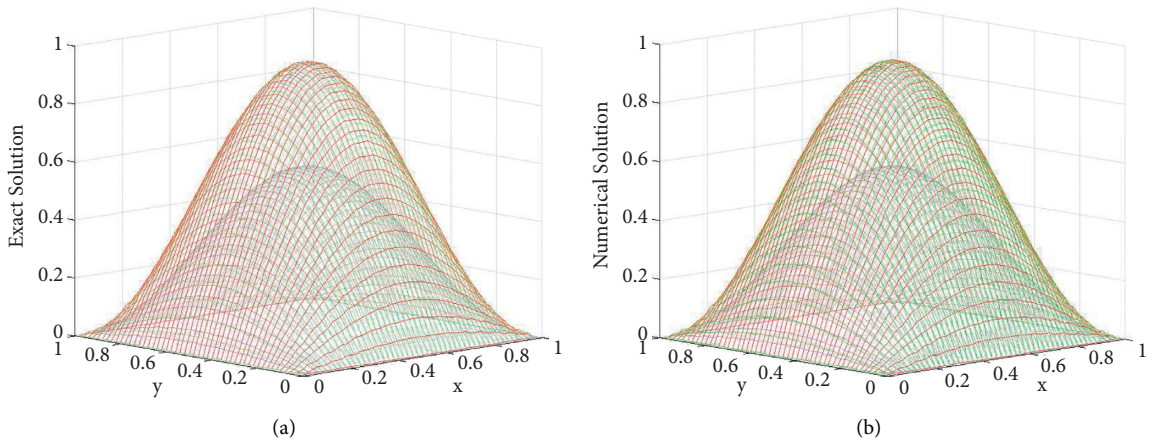

Figure 10: Exact and approximate solutions of problem 2 with $\alpha = 0.1$ and $z = 0.4, 0.6, 0.8$.

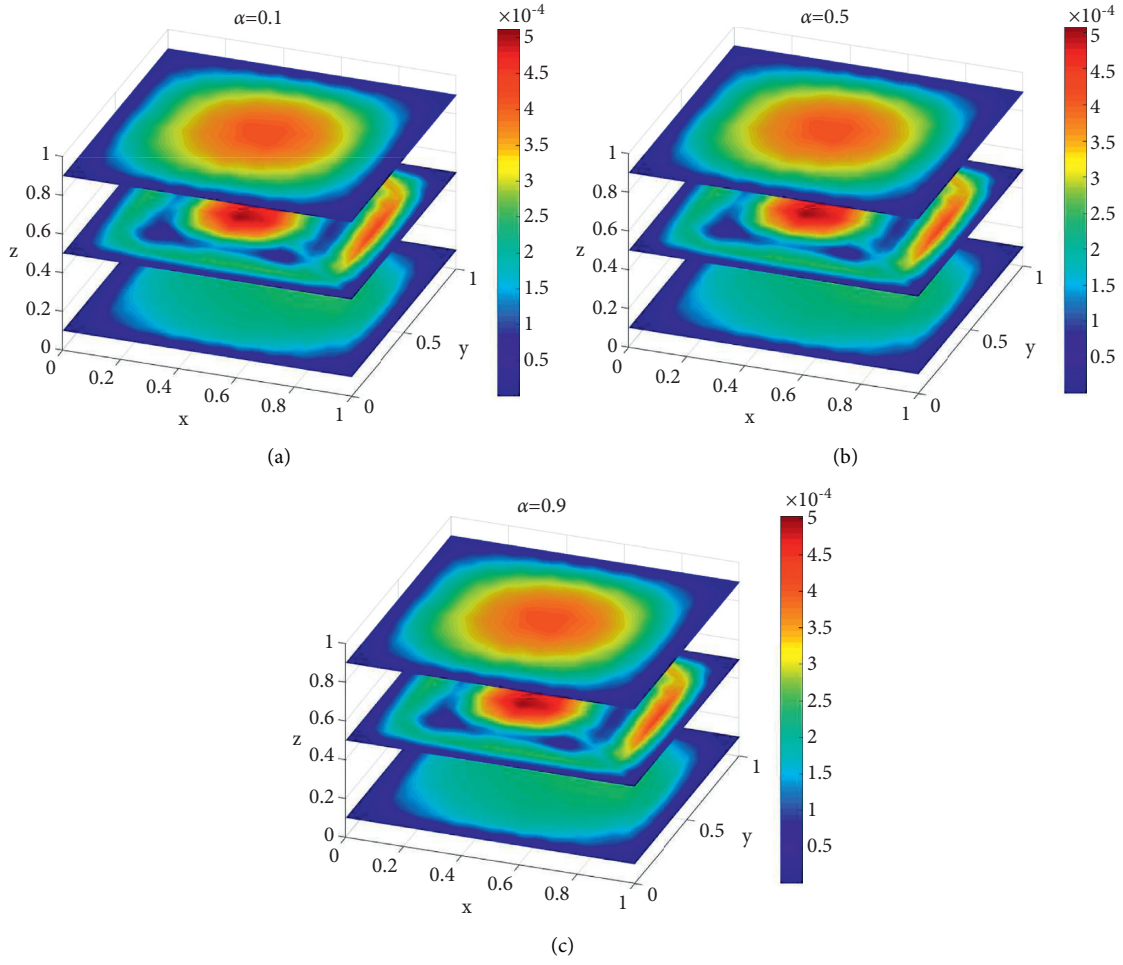

Figure 11: Absolute error in rectangular area using different values of α with $N = 1000$, $n = 75$, and $M = 28$.

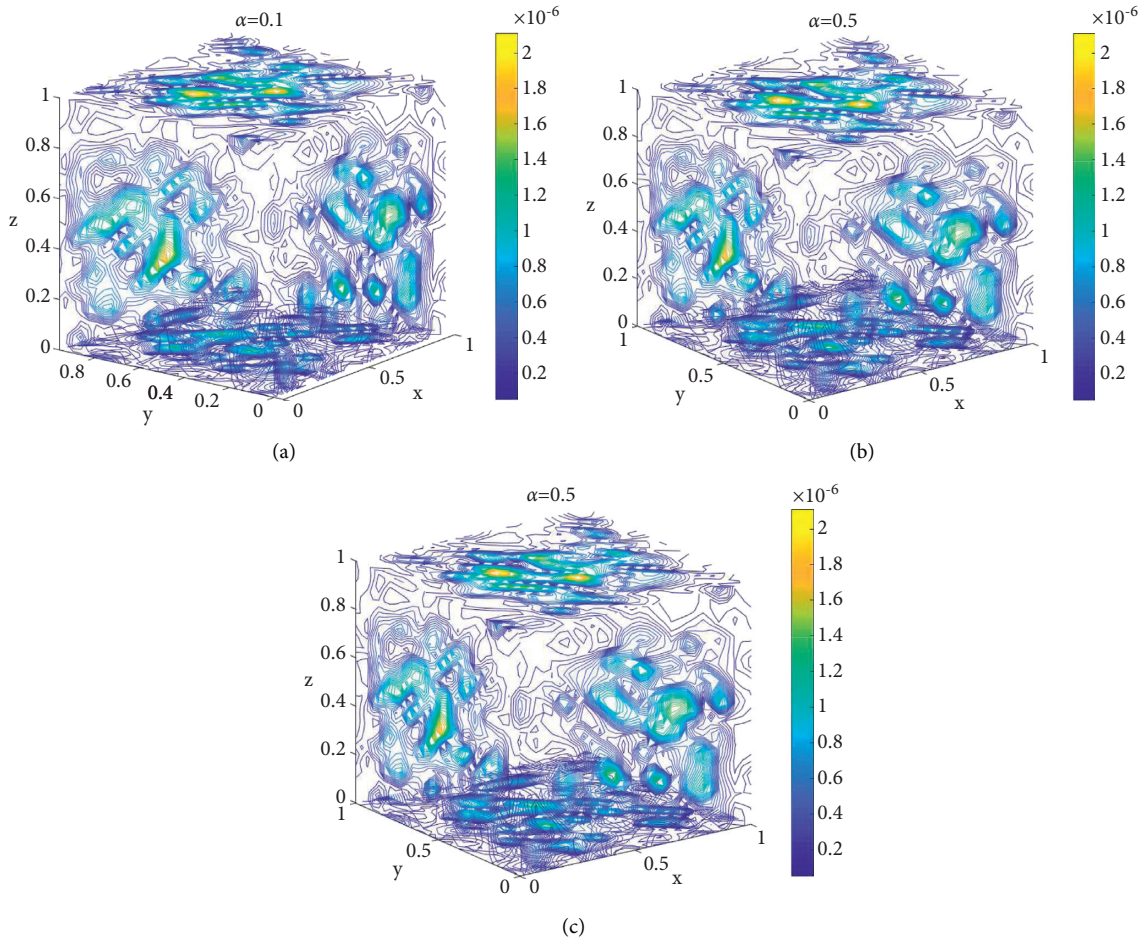

Figure 12: Contour slice of absolute error in rectangular area using different values of α with $N = 4096$, $n = 85$, and $M = 28$.

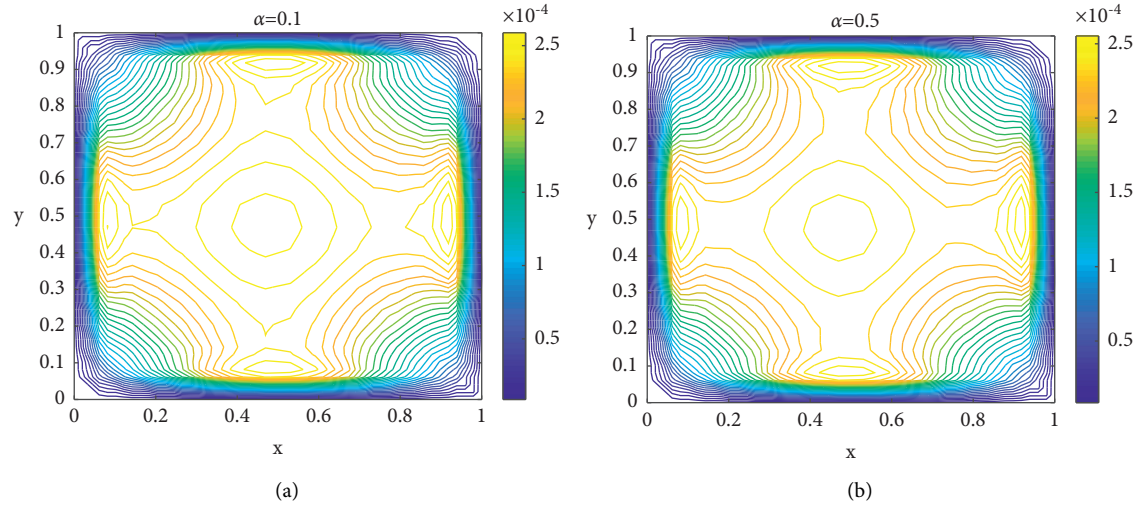

Figure 13: Continued.

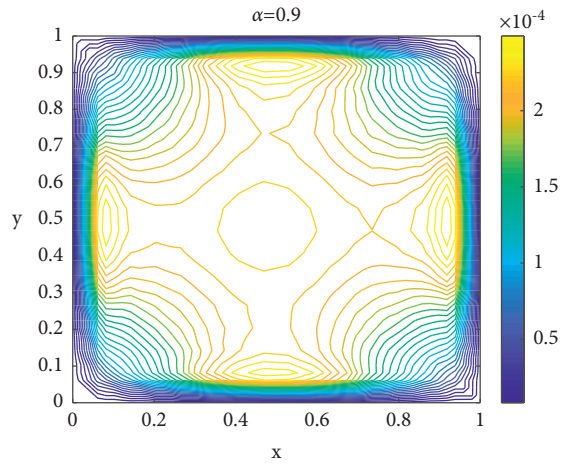

Figure 13: Contour plots of absolute error in rectangular area using different values of α with $N = 256$, $n = 85$, $M = 28$, and $z = 0.5$.

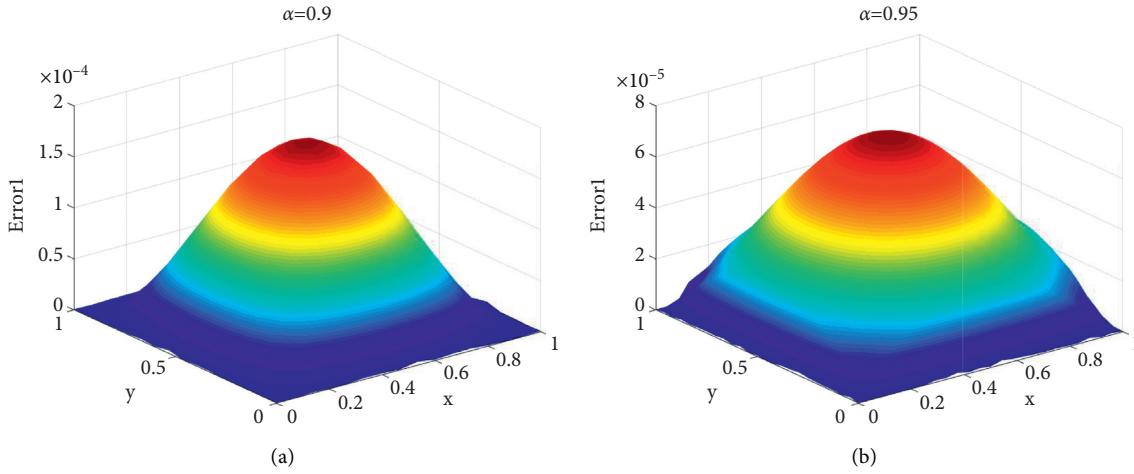

Figure 14: (a) Plot of absolute error with $\alpha = 0.9$, $N = 256$, $n = 25$, $M = 28$, and $z = 0.2$. (b) Plot of absolute error with $\alpha = 0.95$, $N = 625$, $n = 38$, $M = 28$, and $z = 0.8$.

7. Conclusion

In this work, we constructed a method combining LT with the LRBF method for the solution of time fractional CDE in terms of Caputo derivative. The main advantage of this method is obtaining the solution at final time and avoiding the time stepping procedure. The LRBF produced sparse differentiation matrices due to which the ill-conditioning issues of the collocation matrices and the shape parameter's sensitivity were resolved. The convergence of the method was discussed, and the bounds for the stability constant of the fully discrete system were derived. The accuracy of the method was tested by means of two examples, and the results were compared with those from other schemes. The obtained results led us to the conclusion that the proposed method is powerful and effective to find the numerical solutions of three-dimensional time-dependent fractional PDEs, so it can be also applied to a wide range of complex problems that occur in natural sciences and engineering.

Data Availability

The data used to support the findings of this study are included within the article.

Conflicts of Interest

The authors declare that they have no conflicts of interest.

Authors' Contributions

All authors contributed equally to this study.

References

[1] S. G. Samko, A. A. Kilbas, and O. I. Marichev, *Fractional Integrals and Derivatives*, Vol. 1, Gordon and Breach Science Publishers, Yverdon Yverdon-les-Bains, Switzerland, 1993.

[2] A. A. Kilbas, H. M. Srivastava, and J. J. Trujillo, *Theory and Applications of Fractional Differential Equations*, Vol. 204, Elsevier Science Limited, Amsterdam, Netherlands, 2006.

[3] A. A. Alderremy, K. M. Saad, J. F. Gómez-Aguilar, S. Aly, D. Kumar, and J. Singh, "New models of fractional blood ethanol and two-cell cubic autocatalator reaction equations," *Mathematical Methods in the Applied Sciences*, 2021.

[4] B. Cuahutenango-Barro, M. A. Taneco-Hernández, J. F. Gómez-Aguilar, M. S. Osman, H. Jahanshahi, and A. A. Aly, "Analytical solutions of fractional wave equation with memory effect using the fractional derivative with exponential kernel," *Results in Physics*, vol. 25, no. 1, Article ID 104148, 2021.

[5] I. Podlubny, *Fractional Differential Equations: An Introduction to Fractional Derivatives, Fractional Differential Equations, to Methods of Their Solution and Some of Their Applications*, Elsevier, Amsterdam, Netherlands, 1998.

[6] K. B. Oldham and J. Spanier, *The Fractional Calculus Theory and Applications of Differentiation and Integration to Arbitrary Order*, Vol. 111, Academic Press, New York, NY, USA, 1974.

[7] I. Podlubny, "Geometric and physical interpretation of fractional integration and fractional differentiation," arXiv preprint math/0110241, 2001.

[8] P. Zhuang, F. Liu, V. Anh, and I. Turner, "New solution and analytical techniques of the implicit numerical method for the anomalous subdiffusion equation," *SIAM Journal on Numerical Analysis*, vol. 46, no. 2, pp. 1079–1095, 2008.

[9] C.-M. Chen, F. Liu, V. Anh, and I. Turner, "Numerical schemes with high spatial accuracy for a variable-order anomalous subdiffusion equation," *SIAM Journal on Scientific Computing*, vol. 32, no. 4, pp. 1740–1760, 2010.

[10] R. Metzler and J. Klafter, "The random walk's guide to anomalous diffusion: a fractional dynamics approach," *Physics Reports*, vol. 339, no. 1, pp. 1–77, 2000.

[11] Ö. Oruç, "A radial basis function finite difference (RBF-FD) method for numerical simulation of interaction of high and low frequency waves: Zakharov-Rubenchik equations," *Applied Mathematics and Computation*, vol. 394, Article ID 125787, 2021.

[12] A. Golbabai, O. Nikan, and T. Nikazad, "Numerical investigation of the time fractional mobile-immobile advection-dispersion model arising from solute transport in porous media," *International Journal of Algorithms, Computing and Mathematics*, vol. 5, no. 3, p. 50, 2019.

[13] H. Zhang, F. Liu, M. S. Phanikumar, and M. M. Meerschaert, "A novel numerical method for the time variable fractional order mobile-immobile advection-dispersion model," *Computers & Mathematics with Applications*, vol. 66, no. 5, pp. 693–701, 2013.

[14] A. Mohebbi, M. Abbaszadeh, and M. Dehghan, "Solution of two-dimensional modified anomalous fractional sub-diffusion equation via radial basis functions (RBF) meshless method," *Engineering Analysis with Boundary Elements*, vol. 38, pp. 72–82, 2014.

[15] M. M. Khader, K. M. Saad, D. Baleanu, and S. Kumar, "A spectral collocation method for fractional chemical clock reactions," *Computational and Applied Mathematics*, vol. 39, no. 4, pp. 1–12, 2020.

[16] K. M. Saad, M. Alqhtani, and M. Alqhtani, "Numerical simulation of the fractal-fractional reaction diffusion equations with general nonlinear," *AIMS Mathematics*, vol. 6, no. 4, pp. 3788–3804, 2021.

[17] L. J. Chen, M. Li, and Q. Xu, "Sinc-galerkin method for solving the time fractional convection–diffusion equation with variable coefficients," *Advances in Difference Equations*, vol. 2020, no. 1, pp. 1–16, 2020.

[18] R. Hilfer, *Applications of Fractional Calculus in Physics*, World Scientific, Singapore, 2000.

[19] A. Chang, H. Sun, C. Zheng et al., "A time fractional convection-diffusion equation to model gas transport through heterogeneous soil and gas reservoirs," *Physica A: Statistical Mechanics and Its Applications*, vol. 502, pp. 356–369, 2018.

[20] I. M. Sokolov, J. Klafter, and A. Blumen, "Fractional kinetics," *Physics Today*, vol. 55, no. 11, pp. 48–54, 2002.

[21] R. F. Sincovec and N. K. Madsen, "Software for nonlinear partial differential equations," *ACM Transactions on Mathematical Software*, vol. 1, no. 3, pp. 232–260, 1975.

[22] V. F. Morales-Delgado, J. F. Gómez-Aguilar, and M. A. Taneco-Hernandez, "Analytical solution of the time fractional diffusion equation and fractional convection-diffusion equation," *Revista Mexicana de Física*, vol. 65, no. 1, pp. 82–88, 2019.

[23] S. Momani, "An algorithm for solving the fractional convection-diffusion equation with nonlinear source term," *Communications in Nonlinear Science and Numerical Simulation*, vol. 12, no. 7, pp. 1283–1290, 2007.

[24] S. Momani and A. Yıldırım, "Analytical approximate solutions of the fractional convection-diffusion equation with nonlinear source term by He's homotopy perturbation method," *International Journal of Computer Mathematics*, vol. 87, no. 5, pp. 1057–1065, 2010.

[25] Z. Wang and S. Vong, "Compact difference schemes for the modified anomalous fractional sub-diffusion equation and the fractional diffusion-wave equation," *Journal of Computational Physics*, vol. 277, pp. 1–15, 2014.

[26] F. Zeng, C. Li, F. Liu, and I. Turner, "The use of finite difference/element approaches for solving the time-fractional subdiffusion equation," *SIAM Journal on Scientific Computing*, vol. 35, no. 6, pp. A2976–A3000, 2013.

[27] A. Hussain, Z. Zheng, and E. F. Anley, "Numerical analysis of convection-diffusion using a modified upwind approach in the finite volume method," *Mathematics*, vol. 8, no. 11, p. 1869, 2020.

[28] V. Shankar, "The overlapped radial basis function-finite difference (RBF-FD) method: a generalization of RBF-FD," *Journal of Computational Physics*, vol. 342, pp. 211–228, 2017.

[29] M. Dehghan and N. Shafieeabyaneh, "Local radial basis function–finite-difference method to simulate some models in the nonlinear wave phenomena: regularized long-wave and extended Fisher-Kolmogorov equations," *Engineering with Computers*, vol. 37, pp. 1159–1179, 2021.

[30] S. Wei, W. Chen, and Y. C. Hon, "Implicit local radial basis function method for solving two-dimensional time fractional diffusion equations," *Thermal Science*, vol. 19, no. suppl. 1, pp. 59–67, 2015.

[31] Q. Xu and J. S. Hesthaven, "Discontinuous Galerkin method for fractional convection-diffusion equations," *SIAM Journal on Numerical Analysis*, vol. 52, no. 1, pp. 405–423, 2014.

[32] X. Zhao and Z.-Z. Sun, "A box-type scheme for fractional subdiffusion equation with Neumann boundary conditions," *Journal of Computational Physics*, vol. 230, no. 15, pp. 6061–6074, 2011.

[33] J. Hristov, "Approximate solutions to fractional subdiffusion equations," *The European Physical Journal—Special Topics*, vol. 193, no. 1, pp. 229–243, 2011.

[34] S. Zhai, X. Feng, and Y. He, "An unconditionally stable compact ADI method for three-dimensional time-fractional convection-diffusion equation," *Journal of Computational Physics*, vol. 269, pp. 138–155, 2014.

[35] F. Zeng, C. Li, F. Liu, and I. Turner, "Numerical algorithms for time-fractional subdiffusion equation with second-order accuracy," *SIAM Journal on Scientific Computing*, vol. 37, no. 1, pp. A55–A78, 2015.

[36] Y.-N. Zhang and Z.-Z. Sun, "Alternating direction implicit schemes for the two-dimensional fractional sub-diffusion equation," *Journal of Computational Physics*, vol. 230, no. 24, pp. 8713–8728, 2011.

[37] J. Ren, Z.-Z. Sun, and X. Zhao, "Compact difference scheme for the fractional sub-diffusion equation with Neumann boundary conditions," *Journal of Computational Physics*, vol. 232, no. 1, pp. 456–467, 2013.

[38] G.-H. Gao and Z.-Z. Sun, "A compact finite difference scheme for the fractional sub-diffusion equations," *Journal of Computational Physics*, vol. 230, no. 3, pp. 586–595, 2011.

[39] M. Dehghan, M. Abbaszadeh, and A. Mohebbi, "Error estimate for the numerical solution of fractional reaction–subdiffusion process based on a meshless method," *Journal of Computational and Applied Mathematics*, vol. 280, pp. 14–36, 2015.

[40] H. Brunner, L. Ling, and M. Yamamoto, "Numerical simulations of 2D fractional subdiffusion problems," *Journal of Computational Physics*, vol. 229, no. 18, pp. 6613–6622, 2010.

[41] S. Wei, W. Chen, Y. Zhang, H. Wei, and R. M. Garrard, "A local radial basis function collocation method to solve the variable-order time fractional diffusion equation in a two-dimensional irregular domain," *Numerical Methods for Partial Differential Equations*, vol. 34, no. 4, pp. 1209–1223, 2018.

[42] E. Shivanian, "Local radial basis function interpolation method to simulate 2D fractional-time convection-diffusion-reaction equations with error analysis," *Numerical Methods for Partial Differential Equations*, vol. 33, no. 3, pp. 974–994, 2017.

[43] S. A. Sarra, "A local radial basis function method for advection-diffusion-reaction equations on complexly shaped domains," *Applied Mathematics and Computation*, vol. 218, no. 19, pp. 9853–9865, 2012.

[44] A. Golbabai and N. Kalarestaghi, "Improved localized radial basis functions with fitting factor for dominated convection-diffusion differential equations," *Engineering Analysis with Boundary Elements*, vol. 92, pp. 124–135, 2018.

[45] X. M. Gu and S. L. Wu, "A parallel-in-time iterative algorithm for Volterra partial integral-differential problems with weakly singular kernel," *Journal of Computational Physics*, vol. 417, Article ID 109576, 2020.

[46] M. D. Buhmann, *Radial Basis Functions: Theory and Implementations*, Vol. 12, Cambridge University Press, Cambridge, UK, 2003.

[47] R. Schaback, "Error estimates and condition numbers for radial basis function interpolation," *Advances in Computational Mathematics*, vol. 3, no. 3, pp. 251–264, 1995.

[48] L. N. Trefethen and D. Bau, *Numerical Linear Algebra*, Vol. 50, SIAM, Philadelphia, PA, USA, 1997.

[49] B. Davies and B. Martin, "Numerical inversion of the Laplace transform: a survey and comparison of methods," *Journal of Computational Physics*, vol. 33, no. 1, pp. 1–32, 1979.

[50] B. Dingfelder and J. A. C. Weideman, "An improved Talbot method for numerical Laplace transform inversion," *Numerical Algorithms*, vol. 68, no. 1, pp. 167–183, 2015.

[51] J. A. C. Weideman, "Optimizing Talbot's contours for the inversion of the Laplace transform," *SIAM Journal on Numerical Analysis*, vol. 44, no. 6, pp. 2342–2362, 2006.

[52] A. Talbot, "The accurate numerical inversion of Laplace transforms," *IMA Journal of Applied Mathematics*, vol. 23, no. 1, pp. 97–120, 1979.

[53] S. A. Sarra and E. J. Kansa, "Multiquadric radial basis function approximation methods for the numerical solution of partial differential equations," *Advances in Computational Mechanics*, vol. 2, no. 2, 2009.

[54] M. H. Srivastava, H. Ahmad, I. Ahmad, P. Thounthong, and M. N. Khan, "Numerical simulation of three-dimensional fractional-order convection-diffusion pdes by a local meshless method," *Thermal Science*, vol. 25, pp. 347–358, 2021.

[55] Y. Qiao, S. Zhai, and X. Feng, "RBF-FD method for the high dimensional time fractional convection-diffusion equation," *International Communications in Heat and Mass Transfer*, vol. 89, pp. 230–240, 2017.